CrystEngComm

Cite this: *CrystEngComm*, 2012, **14**, 7626–7632

www.rsc.org/crystengcomm

**PAPER**

# Monodispersed $FeNi_2$ alloy nanostructures: solvothermal synthesis, magnetic properties and size-dependent catalytic activity†

**Kong-Lin Wu, Rui Yu and Xian-Wen Wei***

***Received 30th March 2012, Accepted 29th June 2012***
**DOI: 10.1039/c2ce25457c**



This article presents the fabrication of size-/shape-controllable monodispersed Fe–Ni alloy nanostructures *via* a facile solvothermal method by the co-reduction of $Fe^{3+}$ and $Ni^{2+}$ with hydrazine hydrate in a strong alkaline media. The products were characterized by X-ray powder diffraction (XRD), scanning electron microscopy (SEM), transmission electron microscopy (TEM), selected area electron diffraction (SAED), energy dispersive X-ray spectroscopy (EDX) and vibrating sample magnetometry (VSM). The sizes and morphologies of the Fe–Ni alloy nanostructures are dependent on the reaction conditions, such as surfactant, solvent, the molar ratio of metal ions and the amount of alkali. Excitingly, the magnetic hysteresis measurements revealed that the $FeNi_2$ alloy nanostructures display ferromagnetic behavior with enhanced magnetic properties at room temperature. In addition, $FeNi_2$ alloy nanoparticles with different sizes were used as reusable heterogeneous catalysts to reduce *p*-nitrophenol (*p*-NP) to *p*-aminophenol (*p*-AP) by $NaBH_4$ in aqueous solution and show a good potential application in the area of chemical catalysis. Furthermore, the Fe–Ni alloy nanoparticles also have potential applications in the fields of magnetic recording devices, biotechnology and environmental treatment.

## Introduction

As an important functional material, magnetic metals and alloys are of great interest due to a variety of useful chemical and physical properties and have potential technological applications in catalysis, high density magnetic storage devices, magnetic fluids, sensors, electromagnetic shielding and absorbing materials and so forth.[1–6] It is well-known that the properties of nanoparticles are strongly dependent on their sizes, shapes and compositions.[7] In recent years, Fe–Ni alloys with controllable sizes, shapes, compositions and morphologies have been successfully prepared by a number of physical and chemical methods. For example, Fe–Ni alloy nanoparticles were synthesized by the thermal decomposition of organometallic precursors,[3a,8] a cryogenic melting technique,[5] electrochemistry,[9] a reverse micelle technique,[10] mechanical alloying,[11] hydrogen reduction,[12] chemical reduction,[13] a template approach,[14] a microwave plasma or sonochemical method[15] and a hydrothermal or solvothermal method.[16] At the same time, the Fe–Ni alloy nanoparticles were investigated as catalysts.[17] For instance, the $Ni_xFe_{1-x}$ alloy nanoparticles can be used as catalysts for the selective synthesis of semiconducting single-walled carbon nanotubes[17a] and for wastewater treatment, such as hydrodechlorination[17b,17c] and degradation azo dye.[17d] Therefore, the controllable synthesis of functional materials such as Fe–Ni alloy nanoparticles is still a challenge.

In the last decade or so, solvothermal methods in pure or a mixture of organic phases has been widely used as the approach of choice for the synthesis of nano/micrometer-scale magnetic metallic or alloy powders.[18] However, it still remains a challenge to prepare iron and its alloyed nanocrystals because iron readily transforms into stable oxides or hydroxides. Therefore, a strong reducing agent, surface catalysis or high-pressure is needed for the reduction of $Fe^{3+}$ and $Fe^{2+}$ in the reaction mixture to avoid the kinetic difficulties.[19] The reduction of iron ions by $KBH_4$ or $NaBH_4$ in an aqueous solution produces various compounds, such as the Fe–B alloy, rather than pure metal or metal alloy nanoparticles.[20] In addition, the products obtained are in an amorphous state and need further annealing.[20] Hydrazine hydrate is an important reducing agent and has been successfully used for the synthesis of a variety of nanoscale metal materials because it has a strong reducing ability, a low concentration of impurities and is low cost.[4a,4b,16a–c,18a–f] The solvothermal method appears to be a very effective process for the controlled synthesis of alloyed nanoparticles because it allows for an almost simultaneous reduction of two metal salts under high temperature and high pressure conditions, under which aqueous or

*College of Chemistry and Materials Science, Key Laboratory of Functional Molecular Solids, the Ministry of Education, Anhui Laboratory of Molecule-based Materials, Anhui Normal University, Wuhu, 241000, P. R. China. E-mail: xwwei@mail.ahnu.edu.cn; Fax: 86 553 3937137; Tel: 86 553 3869301*

† Electronic supplementary information (ESI) available: Size distribution of the Fe–Ni alloy obtained by using different amounts of PVP, SEM images of the Fe–Ni alloy synthesized with different reaction temperatures, times and solvents and the detailed experimental results. See DOI: 10.1039/c2ce25457c

organic solutions exhibit a critical or supercritical state.[4a,21] To the best of our knowledge, Fe–Ni alloys with dendrite,[16a] spherical[16b] and flower-like morphologies[13c,16c] were obtained. However, there have been few reports on the synthesis of Fe–Ni alloy nanocrystallites from hydrazine hydrate through a solvothermal method in organic solvent.

In this work, we describe a facile solvothermal method to synthesize Fe–Ni alloy nanoparticles with different sizes and morphologies by reducing iron and nickel salts with hydrazine hydrate within a strong alkaline media in an organic solvent with a high boiling point. Different experimental parameters were carried out to investigate their effects on the products. The magnetic properties of $FeNi_2$ alloys with different sizes were investigated. The $FeNi_2$ alloy nanoparticles were applied as catalysts in reducing *p*-nitrophenol (*p*-NP) to *p*-aminophenol (*p*-AP) by $NaBH_4$.

## Experimental section

### Synthesis of the Fe–Ni alloys

All the chemicals used in this work were of analytical grade and were used as received without further purification. In a typical procedure, 35 mL of a mixture of $FeCl_3{\cdot}6H_2O$ (0.181 g) and $NiCl_2{\cdot}6H_2O$ (0.317 g) in glycerin, with or without surfactant, was strongly stirred at 50 °C in a water bath for 30 min to ensure that all of the reagents were dispersed homogeneously in the solution. Subsequently, 5 mL of aqueous hydrazine ($N_2H_4{\cdot}H_2O$, 85 wt %) and a sodium hydroxide (NaOH, 0.4 g) solution were added dropwise into the above solution and after being vigorously stirred for 5 min, the mixture was transferred into a Teflon-lined stainless-steel autoclave with a capacity of 60 mL. The autoclave was sealed and put into a furnace, which was heated to and maintained at 180–220 °C for 1–50 h, and then taken out and allowed to cool naturally to room temperature. The final products were collected by magnetic separation, washed with distilled water and ethanol several times under ultrasonic conditions and then dried in a vacuum oven at 60 °C for 5 h. Additionally, we kept the total concentration of metal ions at 0.05 M when other similar experiments were carried out by modulating several parameters, such as the molar ratio of $Fe^{3+}$ to $Ni^{2+}$, the amount of NaOH, the types of surfactant and solvent and the reaction temperature and time (see Table S1, ESI†).

### Characterization

The structural information from the samples was collected by X-ray powder diffraction (XRD) measurements which were carried out on a Shimadzu XRD-6000 X-ray diffractometer (Cu–K$\alpha$ radiation, $\lambda$ = 1.5406 Å) with $2\theta$ values from 20° to 80° at a scanning rate of 0.05° $s^{-1}$. The operation voltage and current were kept at 40 kV and 30 mA, respectively. The chemical composition (atomic percent) of the as-prepared Fe–Ni alloys was determined by energy-dispersive X-ray (EDX) spectrometry (Hitachi S–4800 Japan). The morphologies of the samples were studied by scanning electron microscopy (SEM) (Hitachi S–4800 Japan). Transmission electron microscopy (TEM) and high resolution TEM (HRTEM) were performed using a JEM-2010 microscope operated at 200 kV. Magnetic measurements of the samples were carried out at room temperature using a vibrating sample magnetometer (VSM, BHV-55) with a maximum magnetic field of 5 kOe. Nitrogen adsorption experiments of the as-synthesized samples were measured at 77 K on a Micromeritics ASAP 2020 system. The UV-vis measurements were performed on a U4100 (Hitachi, Japan) spectrophotometer using colloidal suspensions in deionized water.

### Catalytic reaction

In a typical catalytic reaction, 1 mL (1.0 × $10^{-4}$ M) of an aqueous solution of *p*-NP and 1 mL (100 mg $L^{-1}$) of the aqueous $FeNi_2$ alloy colloidal suspensions were mixed together in a 1 cm quartz cuvette and inert $N_2$ was used to remove the dissolved oxygen. Next, 1 mL (6 × $10^{-2}$ M) of an aqueous $NaBH_4$ solution was added to the reaction mixture and time-dependent absorption spectra were recorded on the UV-vis spectrophotometer at 20 °C.

## Results and discussion

### Controlled synthesis of the Fe–Ni alloy nanospheres

The phase structure and purity of the as-synthesized sample was examined by X-ray powder diffraction (XRD). Fig. 1a shows the typical XRD pattern of the products obtained by the reduction of $Fe^{3+}$ and $Ni^{2+}$ in glycerin at 200 °C for 4 h. The peaks at

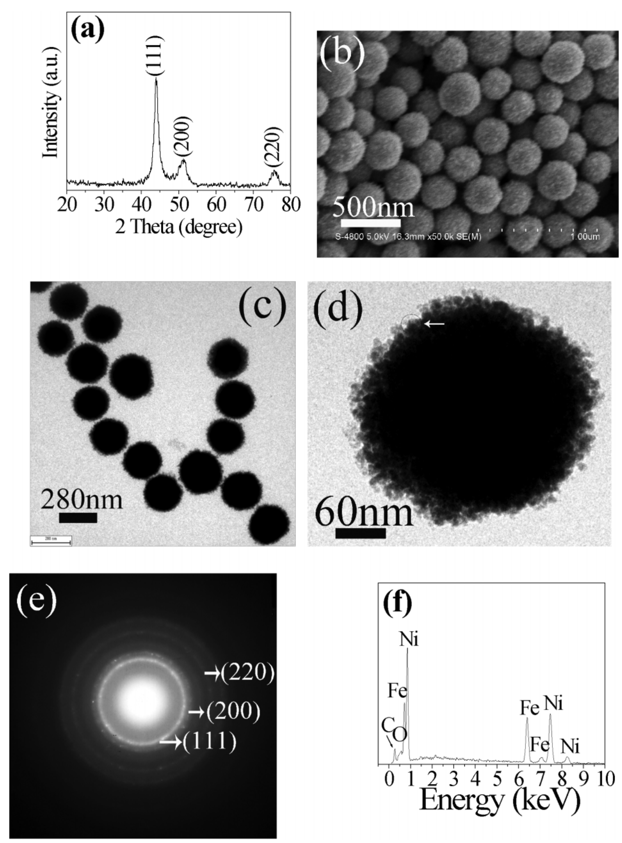


**Fig. 1** Integrated characterization of the Fe–Ni alloy obtained by the reduction of $Fe^{3+}$ and $Ni^{2+}$ with hydrazine in glycerin at 200 °C for 4 h in the absence of PVP. (a) XRD pattern, (b) SEM image, (c) and (d) TEM images, (e) SAED pattern taken from the side of the nanospheres in panel (d) and (f) EDX spectrum taken of the nanospheres in panel (b).

$2\theta$ = 44.16, 51.27 and 75.45° can be easily assigned to the (111), (200) and (220) reflections of the fcc phase of the Fe–Ni alloy (JCPDS No. 38-0419), respectively. It is noted that the (111) peak of the as-obtained Fe–Ni alloy shifts to a lower angle (*ca.* 0.34°) relative to the standard pattern of the pure nickel (JCPDS 04-0850). The lattice constant, *a*, which is calculated from the (111) peak is 3.549 Å, is larger than that of fcc Ni ($a$ = 3.523 Å, JCPDS 04-0850). This implies that the Fe atoms are incorporated into the fcc Ni lattice, leading to the enlargement of the interplanar spacing as the radius of the Fe atoms (1.26 Å) is larger than that of the Ni atoms (1.24 Å).[4b,10a] No iron and nickel oxide or hydroxides or other impurity phases are detected.

The morphology and size of the final products were further examined by scanning electron microscopy (SEM) and transmission electron microscopy (TEM). The low-magnification SEM image (Fig. 1b) reveals that the product is composed of uniform ordered nanospheres in high yield. Fig. 1c and Fig. 1d show the typical TEM images of the as-prepared Fe–Ni alloys. It can be clearly seen that the products contain uniform sphere-like morphologies, which is consistent with the results of the SEM (Fig. 1b). A selected-area electron diffraction (SAED) pattern in Fig. 1e, taken from the edge of the nanosphere in Fig. 1d, reveals the polycrystalline nature of the Fe–Ni alloy nanospheres. The particle diameter of the nanospheres over the whole sample was *ca.* 300 nm, which is in accordance with the size distribution of the nanospheres (Fig. S1a, ESI†). The thin oxidation shell, with a thickness of about 3 nm, can be seen from the HRTEM image (Fig. S2, ESI†). The chemical composition (atomic percent) of these nanospheres was further determined by energy dispersive X-ray (EDX) spectrometry (Fig. 1f) and the only detectable elements are iron, nickel, carbon and oxygen. While the carbon and oxygen should arise from the thin macromolecule film covering the copper grid or from the oxidation surface of the samples, the corresponding elementary analysis reveals that the atomic ratio of Fe to Ni is 34.8 : 65.2, which is very close to the initial set ratio of $Fe^{3+}$ : $Ni^{2+}$ = 1 : 2.

When synthesising magnetic Ni–Co and Fe–Co alloys by a solvothermal method, different experimental parameters could affect the sizes, morphologies and compositions *etc.*[18d–i] Herein, several experiments were also carried out to determine the parameters (such as the type and amount of surfactant, the reaction temperature and time, the amount of NaOH, the types of solvent and the molar ratio of $Fe^{3+}$ to $Ni^{2+}$) that might affect the formation of the Fe–Ni alloy nanostructures (see Table S1, ESI†). It was found that the presence of a surfactant played a crucial role in the formation of Fe–Ni alloy spherical nanostructures. We used cetyltrimethyl ammonium bromide (CTAB, 1 mmol), dodecyl benzene sulfonic acid sodium (SDBS, 1 mmol), polyethylene glycol ($M_w$ = 20 000, 1 mmol) (PEG-20 000) and polyvinylpyrrolidone (PVP, 1 mmol) as examples of different surfactants and SEM images of the products are shown in Fig. 2a–d. In this synthesis process, Fe–Ni alloy nanoparticles with uniform sizes of *ca.* 230 nm (Fig. S1b, ESI†) and spherical nanostructures (Fig. 2d) were obtained in the presence of PVP (1 mmol), whereas perfectly spherical Fe–Ni alloy nanoparticles could not formed by using other surfactants (Fig. 2a–c). The quantity of PVP was also found to have a remarkable influence on the size of the final products. On increasing the amount of PVP from 1 mmol (Fig. 2d) to 2 mmol (SEM image and size distribution are shown in Fig. 2e and Fig. S1c, respectively†), the morphologies were maintained as unchanged spheres but the sizes decreased from *ca.* 230 nm to *ca.* 170 nm. When the amount of PVP was increased to 10 mmol, an Fe–Ni alloy with a spherical morphology was obtained (Fig. 2f) but a broad size distribution could be detected (Fig. S1d, ESI†). In addition, the SEM results show that the reaction temperatures (Fig. S3, ESI†) very weakly affect the morphologies of the products in the absence of PVP, so we choose 200 °C as the reaction temperature since the yield is higher than that at 180 °C. It was found that the reaction time is important for the synthesis of Fe–Ni alloys (Fig. S4, ESI†) because if the reaction time was too short *i.e.* 1 h, then irregular spherical structures were obtained. As the time increased to 10, 20 or 50 h, mixed structures of nanospheres and nanofibres were attained. Consequently, the best reaction time for preparing Fe–Ni alloys is 4 h in this system. Therefore, we can control the amount of PVP to fabricate $FeNi_2$ alloy nanospheres with different sizes.

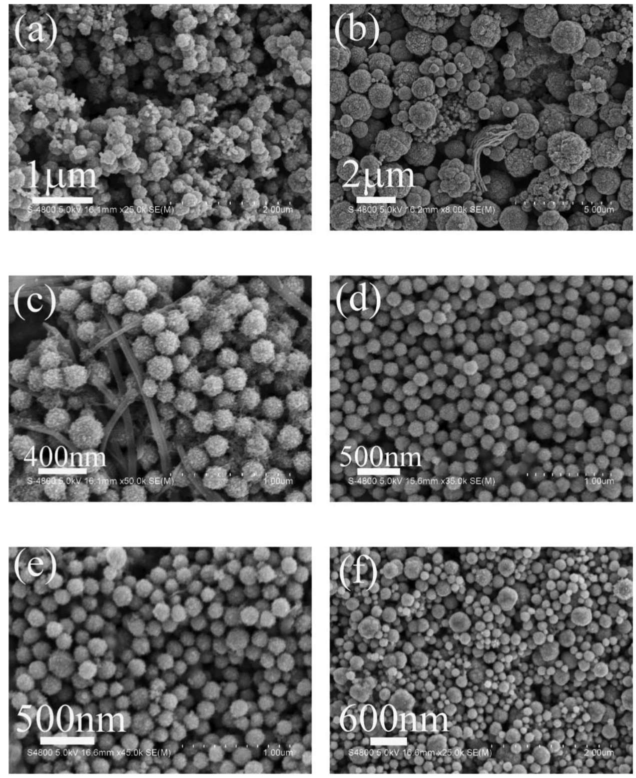


**Fig. 2** SEM images of the Fe–Ni crystals formed by using different surfactants: (a) CTAB (1 mmol), (b) SDBS (1 mmol), (c) PEG-20 000 (1 mmol), (d) PVP (1 mmol), (e) PVP (2 mmol) and (f) PVP (10 mmol) whilst keeping the other conditions the same.

We know that the pH value is a key factor to persuade the reducing $Ni^{2+}$, $Co^{2+}$ or $Cu^{2+}$ ions to their alloys.[18a] It was found that NaOH also plays an important role in the synthesis of the $FeNi_2$ alloy nanoparticles (Fig. 3). It is known that a basic medium could improve the reducing power of hydrazine[22a] and without NaOH, no Fe–Ni alloys were obtained. When the concentration of NaOH was 0.125 M, very few products and irregular particles were attained (Fig. 3a). Increasing the concentration of NaOH (0.25 M and 0.375 M) in the mixture led to the formation of well-defined $FeNi_2$ alloy nanospheres

 

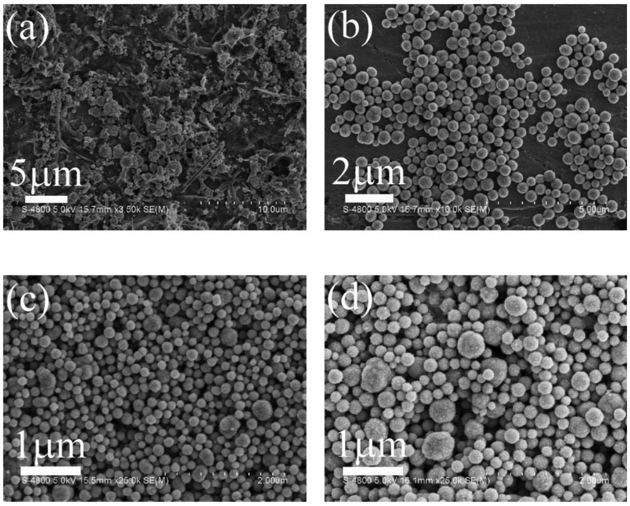


**Fig. 3** SEM images of the Fe–Ni crystals obtained with different concentrations of NaOH whilst keeping the other conditions constant: (a) 0.125 M, (b) 0.375 M, (c) 0.5 M and (d) 0.75 M.

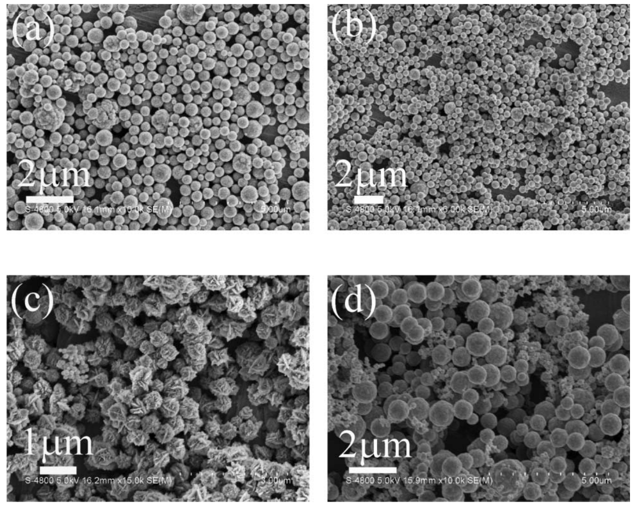


**Fig. 4** SEM images of the Fe–Ni crystals synthesized at various initial ratios of $Fe^{3+}$ to $Ni^{2+}$ whilst keeping other conditions the same: (a) 50 : 50, (b) 25 : 75, (c) 20 : 80 and (d) 0 : 100.

(Fig. 1b and Fig. 3b). As the concentration of NaOH was further increased (0.5 M and 0.75 M), the final products were dominated by irregular nanospheres (Fig. 3c and Fig. 3d). Consequently, the metal crystal growth rate was correspondingly increased by increasing the alkali concentration. A similar phenomenon was also revealed in the formation of Co[22b] and $FeNi_3$[16a] dendrites. Therefore, the best NaOH concentration is in the range of 0.25–0.375 M.

The viscosity and coordinating ability of the solvents can be attributed to the effects of the reaction rate, size, phase and the morphology of the metal or alloy nanomaterials.[18d,22c] In order to fully understand the role of the solvents on the morphologies of the products, a series of experiments with different solvents were performed, for example, *n*-propyl alcohol (NPA), ethylene glycol (EG) and 1,3-dihydroxypropane (DPE) were used. The SEM images of the samples obtained are shown in Fig. S5.† When the glycerin was substituted with NPA, the environment did not favor the formation of nanosphere structures but imperfect nanoparticles with a wide size distribution (Fig. S5a, ESI†). When EG was used, nanospheres with enhanced sizes were formed and self-assembled into chain-like structures by dipole-directed interactions (Fig. S5b, ESI†).[18e,18f] Finally, when DPE was used, mixtures of nanosphere and nanoflower-like were produced (Fig. S5c, ESI†). The viscosity ranking of the four different solvents is NPA < EG < PDE < glycerin. Thereby, to some extent, higher viscosity can slow down the growth rate and be more advantageous for isotropic growth.[17c,22c,23] EG and PDE, having high viscosities, largely restrain the diffusion of the Fe–Ni nuclei and only result in spherical nanoparticles, similar to Zhu's work[22c] and our very recent work.[18d] Hence, the glycerin provides a good environment for the growth of uniform spherical Fe–Ni alloy nanostructures.

The initial ratio of the different metal ions was also found to have a remarkable influence on the size, morphology and composition of the final products.[18d] Herein, we kept the total metal ion concentration and other parameters constant while Fe–Ni crystals with varying Fe concentrations were synthesized using a specific ratio of $Fe^{3+}$ and $Ni^{2+}$ salts in the absence of PVP in glycerin at 200 °C for 4 h. The initial ion composition, the final composition and the morphology of the Fe–Ni crystals obtained are shown in Table S1 (ESI†). SEM images of the Fe–Ni crystals with different initial ratios of $Fe^{3+}$ to $Ni^{2+}$ are shown in Fig. 4. The shape of the Fe–Ni crystals with different compositions varied from irregular spheres (Fig. 4a–b) to flower-like (Fig. 4c) then chain-like (Fig. 4d) structures when they were rich in Ni. In our system, the initial ratio of $Fe^{3+}$ to $Ni^{2+}$ changed from 50 : 50 to 25 : 75, the Fe–Ni crystals assume spherical shapes. When the initial ratio is 20 : 80, Fe–Ni crystals assume a flower-like structure. While the initial ratio is 0 : 100, pure Ni nanospheres were obtained. In particular, very few Fe–Ni crystals were obtained when the initial ratio of $Fe^{3+}$ to $Ni^{2+}$ is Fe-enriched. The results revealed that more Fe-enriched alloys can not be obtained when using glycerin as the organic solvent because not enough power is provided under these conditions to avoid the kinetic difficulties.

When Fe(III) and Ni(II) are treated with hydrazine hydrate in an alkaline medium, $Fe(OH)_3$ is easily formed under these basic conditions. Ni(II) coordinated with hydrazine is readily reduced to Ni(0) particles, which in turn reduces $Fe(OH)_3$ to Fe(0) particles as a surface catalyst.[19a] In our experiment, the molar ratio of $Fe^{3+}$ to $Ni^{2+}$ is equal to 1 : 2 and $Fe^{3+}$ and $Ni^{2+}$ can be completely reduced to Fe and Ni, resulting in the formation of fcc $FeNi_2$. Due to the minimization of the surface free energy and the strong magnetic dipole–dipole interaction,[24,25] spherical nanoparticles formed *via* the random aggregation of the newly formed nuclei. Based on a precipitate slow-release controlled process,[22b] $Fe^{3+}$ and $Ni^{2+}$ can be slow-released from $Fe(OH)_3$ and $Ni(OH)_2$ by high temperature decomposition in solvothermal conditions. As a result, the concentrations of $Fe^{3+}$ and $Ni^{2+}$ are maintained at a stable level. Faster growth leads to a similar growth rate of various facets and isotropic morphology, *e.g.*, spheres are usually obtained.

### Magnetic properties of Fe–Ni alloys

The magnetic properties of the spherical Fe–Ni crystals with different sizes have been investigated at room temperature using

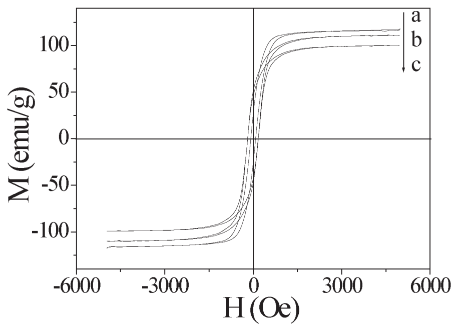


**Fig. 5** Hysteresis loops of the Fe–Ni crystals with different sizes: (a) *ca.* 300 nm, (b) *ca.* 230 nm, and (c) *ca.* 170 nm.

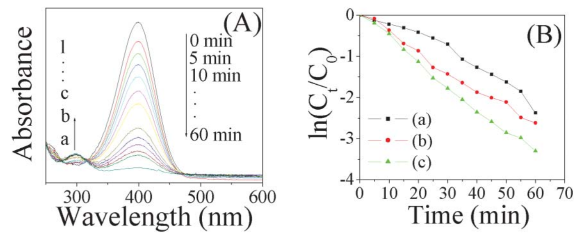


**Fig. 6** (A) Time-dependent UV-vis spectral changes in the reaction mixture catalyzed by Fe–Ni crystals with sizes of *ca.* 300 nm. Conditions: [4-NP] = 1.0 × $10^{-4}$ M; [$NaBH_4$] = 6.0 × $10^{-2}$ M; Fe–Ni alloy = 100m g $L^{-1}$; the temperature is 20 °C. (B) Plot of $\ln(C_t/C_0)$ *versus* time for each of the Fe–Ni alloys as catalysts with different sizes: (a) *ca.* 300 nm, (b) *ca.* 230 nm, (c) *ca.* 170 nm, respectively.

a vibrating sample magnetometer with an applied field of $-5$ kOe $< H <$ 5 kOe, respectively. The hysteresis loops of the Fe–Ni crystals are shown in Fig. 5 and exhibit ferromagnetic behavior. The saturation magnetization (*M*s), remnant magnetization (*M*r) and coercivity (*H*c) values for the Fe–Ni crystals are shown in Table 1. The *M*s value of the $Fe_{34.8}Ni_{65.2}$ nanospheres (116.5 emu $g^{-1}$, Fig. 5a) with sizes of *ca.* 300 nm is higher than that of the $Fe_{34.1}Ni_{65.9}$ nanospheres (110.1 emu $g^{-1}$, Fig. 5b) with sizes of *ca.* 230 nm and that of the $Fe_{33.5}Ni_{66.5}$ nanospheres (100.2 emu $g^{-1}$, Fig. 5c) with sizes of *ca.* 170 nm. It is also higher than that of the $Fe_{35}Ni_{65}$ alloy nanoparticles (89 emu $g^{-1}$).[3a] The increased *M*s is attributed to the incorporation of Fe atoms, which have higher magnetic moments than Ni atoms.[3a] On the other hand, the *H*c is increased when the size of the Fe–Ni alloy is decreased. Compared to the *H*c of the $FeNi_2$ crystals with sizes of *ca.* 300 nm (84.2 Oe) and *ca.* 230 nm (183.1 Oe), the $Fe_{33.5}Ni_{66.5}$ alloy with sizes of *ca.* 170 nm exhibited an enhanced value (204.1 Oe), which is also higher than that of the $Fe_{35}Ni_{65}$ nanoparticles (103 Oe).[3a] All the *H*c values are superior to those of Fe (∼1 Oe), Ni (∼6 Oe) and the $Fe_xNi_{100-x}$ (< 1 Oe) bulk materials.[26] The larger coercivity of the $Fe_{33.5}Ni_{66.5}$ nanospheres is considered to be attributable to the intrinsic large magnetocrystalline anisotropy of ordered intermetallic compounds and is also mainly due to the effect of the size, shape and structure.[16a] However, these are not the only parameters that we have to consider. The composition, internal stress and defects also influence this value, which needs to be investigated further.

### Catalytic properties of $FeNi_2$ crystals with different sizes

It is well-known that the properties of nanoparticles are strongly dependent on their sizes.[7a–e] Herein, we used Fe–Ni alloys with different sizes as catalysts in a model reaction based on the reduction of *p*-nitrophenol (*p*-NP) to *p*-aminophenol (*p*-AP) by $NaBH_4$. In the absence of catalysts, the *p*-NP can not be reduced by $NaBH_4$ for a couple of days. Previous studies have shown that dissolved oxygen in the aqueous solution may react with $NaBH_4$ first during the *p*-NP reduction, which might cause a time delay in the real reaction. Therefore, the use of an inert gas such as $N_2$ to remove the dissolved oxygen in the aqueous solution is needed before testing.[27] Fig. 6A shows a typical UV-vis absorption change in the reaction mixture through the addition of $Fe_{34.8}Ni_{65.2}$ alloy spheres with diameters of *ca.* 300 nm at 20 °C. In these spectra, the absorption of *p*-NP at 400 nm decreases with a concomitant increase in the 300 nm peak of *p*-AP[7e,7g,28] within 1 h after the addition of the catalyst. Since excess $NaBH_4$ was used, the $BH_4^-$ concentration remained essentially constant throughout the reaction. The UV-vis spectra also exhibits an isosbestic point between the two absorption bands, indicating that only two principal species, *p*-NP and *p*-AP, influence the reaction kinetics.[28a] Therefore, pseudo-first-order kinetics could be applied for the evaluation of rate constants.[7e,7g,28]

Herein, Fe–Ni alloy nanoparticles with different sizes (*ca.* 300 nm, 230 nm and 170 nm) carried out the catalytic reaction of *p*-NP into *p*-AP. In each reaction, the same concentration of catalyst was used. With the different sizes of Fe–Ni alloys, the ratio of $C_t$ and $C_0$, where $C_t$ and $C_0$ are *p*-NP concentrations at time *t* and *0*, respectively, was measured from the relative intensity of the respective absorbances at 400 nm, $A_t/A_0$.[7e,28a] Approximately linear relations between $\ln(C_t/C_0)$ *versus* time were observed for all the catalysts, indicating that the reactions followed pseudo-first-order kinetics. The rate constants were also estimated from diffusion-coupled first order reaction kinetics using the slopes of straight lines in Fig. 6B. The rate constants varied from 6.3 × $10^{-4}$ to 9.5 × $10^{-4}$ $s^{-1}$ (Table 2) as the Fe–Ni alloy diameters decreased from *ca.* 300 to *ca.* 170 nm, which indicated the highest catalytic activity was for the $Fe_{33.5}Ni_{66.5}$ alloy nanospheres with diameters of *ca.* 170 nm, as they have the largest surface-to-volume ratio and surface areas under nearly the same compositions, since the Brunauer-Emmett-Teller (BET) surface areas were determined as 43.22 $m^2$ $g^{-1}$ for the $Fe_{33.5}Ni_{66.5}$ alloy nanospheres with diameters of *ca.* 170 nm, 38.69 $m^2$ $g^{-1}$ for the $Fe_{34.1}Ni_{65.9}$ alloy nanospheres with diameters of *ca.* 230 nm and 27.06 $m^2$ $g^{-1}$ for the $Fe_{34.8}Ni_{65.2}$ alloy nanospheres with diameters of *ca.* 300 nm, respectively. Typically,

**Table 1** Magnetic data of the as-obtained Fe–Ni crystals with different sizes

| Samples | Composition | Size | Ms (emu $g^{-1}$) | Mr (emu $g^{-1}$) | Mr/Ms | *H*c (Oe) |
|---|---|---|---|---|---|---|
| a | $Fe_{34.8}Ni_{65.2}$ | *ca.* 300 nm | 116.5 | 26.8 | 0.23 | 84.2 |
| b | $Fe_{34.1}Ni_{65.9}$ | *ca.* 230 nm | 110.1 | 46.2 | 0.42 | 183.1 |
| c | $Fe_{33.5}Ni_{66.5}$ | *ca.* 170 nm | 100.2 | 45.4 | 0.46 | 204.1 |

 

**Table 2** Rate constants for the reduction of *p*-nitrophenol by Fe–Ni crystals with different sizes and surface areas

| Sample composition | Diameter (nm) | BET surface areas ($m^2 g^{-1}$) | rate constant ($s^{-1}$) |
|---|---|---|---|
| $Fe_{34.8}Ni_{65.2}$ | *ca.* 300 | 27.06 | $6.3 \times 10^{-4}$ |
| $Fe_{34.1}Ni_{65.9}$ | *ca.* 230 | 38.69 | $7.5 \times 10^{-4}$ |
| $Fe_{33.5}Ni_{66.5}$ | *ca.* 170 | 43.22 | $9.5 \times 10^{-4}$ |

a smaller nanoparticle tends to show a higher catalytic activity as it has a much greater surface-to-volume ratio.[7e] This size dependence has been validated in a number of systems.[7b–e] Herein, we believe that the high activity of smaller particles originates from their large surface-to-volume ratio[7e] and surface roughness,[28a] observed in the SEM images (Fig. 1b, Fig. 2d and Fig. 2e, respectively). The catalytic rate constants are not very good, which is attributable to the minor oxidation on the surface of the samples. However, the use of Fe–Ni alloys instead of noble-metals as potential catalysts for the catalytic reduction of *p*-NP to *p*-AP needs further investigation.

## Conclusions

In conclusion, we reported a solvothermal method to synthesize Fe–Ni alloy nanostructures in organic solvents. The size and morphology of the Fe–Ni alloy nanostructures can be controlled by adjusting the ratio of metal ions, the kinds of surfactant and solvent, the amount of surfactant and NaOH *etc.* Magnetic measurements revealed that the $Fe_{34.8}Ni_{65.2}$ alloy with sizes of *ca.* 300 nm has a higher saturation magnetization value (116.5 emu $g^{-1}$) than that of $Fe_{34.1}Ni_{65.9}$ with sizes of *ca.* 230 nm (110.1 emu $g^{-1}$) and $Fe_{33.5}Ni_{66.5}$ with sizes of *ca.* 170 nm (100.2 emu $g^{-1}$), and that $Fe_{33.5}Ni_{66.5}$, with sizes of *ca.* 170 nm, exhibits an enhanced coercivity value. We have demonstrated the $FeNi_2$ alloys with different sizes can be used as new reusable heterogeneous catalysts for the reduction of *p*-nitrophenol by $NaBH_4$ and the rate constants exhibited size-dependent catalytic properties: $Fe_{33.5}Ni_{66.5}$ nanospheres (*ca.* 170 nm) are catalytically more active than both the $Fe_{34.1}Ni_{65.9}$ nanospheres (*ca.* 230 nm) and $Fe_{34.8}Ni_{65.2}$ nanospheres (*ca.* 300 nm). Given the ferromagnetism and abundance as well as the simplicity in controlling the compositions, morphologies and structures, the Fe–Ni alloy nanostructures might have widespread uses as magnetic recording devices and catalysts in a number of industry applications.

## Acknowledgements

This work is supported by the Science and Technological Fund of Anhui Province for Outstanding Youth (No. 08040106906), the National Natural Science Foundation (Nos. 21071005, 20490217, 20671002) of the P. R. of China, the State Education Ministry (EYTP, SRF for ROCS, SRFDP 20070370001), the Education Department (Nos. 2006KJ006TD, 2008Z028) of Anhui Province and the Research Culture Funds of Anhui Normal University (No. 2011rcpy038, 2010rcpy040).

## References


1 M. V. Schilfgaarde, I. A. Abrikosov and B. Johansson, *Nature*, 1999, **400**, 46.
2 (*a*) L. Bouhouch, M. Fadel and E. Hilali, *Phys. Status Solidi C*, 2006, **3**, 3253; (*b*) R. Bolsoni, V. Drago and E. L. Jr, *J. Metastable Nanocryst. Mater.*, 2002, **14**, 51; (*c*) S. Kumar, K. Roy, K. Maity, T. P. Sinha, D. Banerjee, K. C. Das and R. Bhattacharya, *Phys. Status Solidi A*, 1998, **167**, 175.
3 (*a*) Y. Chen, X. Luo, G. H. Yue, X. Luo and D. L. Peng, *Mater. Chem. Phys.*, 2009, **113**, 412; (*b*) A. Datta, M. Pal, D. Chakravorty, D. Das and S. N. Chintalapudi, *J. Magn. Magn. Mater.*, 1999, **205**, 301; (*c*) S. U. Jen, S. P. Shieh and S. S. Liou, *J. Magn. Magn. Mater.*, 1995, **147**, 49.
4 (*a*) Q. L. Liao, R. Tannenbaum and Z. L. Wang, *J. Phys. Chem. B*, 2006, **110**, 14262; (*b*) L. Liu, J. Guan, W. Shi, Z. Sun and J. Zhao, *J. Phys. Chem. C*, 2010, **114**, 13565; (*c*) R. Ferrando, J. Jellinek and R. L. Johnston, *Chem. Rev.*, 2008, **108**, 845.
5 M. Ammar, F. Mazaleyrat, J. P. Bonnet, P. Audebert, A. Brosseau, G. Wang and Y. Champion, *Nanotechnology*, 2007, **18**, 285606.
6 (*a*) A. H. Lu, E. L. Salabas and F. Schüth, *Angew. Chem., Int. Ed.*, 2007, **46**, 1222; (*b*) T. D. Schladt, K. Schneider, H. Schildb and W. Tremel, *Dalton Trans.*, 2011, **40**, 6315.
7 (*a*) A. P. Alivisatos, *Science*, 1996, **271**, 933; (*b*) M. A. El-Sayed, *Acc. Chem. Res.*, 2001, **34**, 257; (*c*) M. C. Daniel and D. Astruc, *Chem. Rev.*, 2004, **104**, 293; (*d*) B. K. Min and C. M. Friend, *Chem. Rev.*, 2007, **107**, 2709; (*e*) J. Zeng, Q. Zhang, J. Chen and Y. Xia, *Nano Lett.*, 2010, **10**, 30; (*f*) R. Narayanan and M. A. EI-Sayed, *Nano Lett.*, 2004, **4**, 1343; (*g*) S. K. Ghosh, M. Mandal, S. Kundu, S. Nath and T. Pal, *Appl. Catal., A*, 2004, **268**, 61.
8 I. Robinson, S. Zacchini, L. D. Tung, S. Maenosono and N. T. K. Thanh, *Chem. Mater.*, 2009, **21**, 3021.
9 (*a*) S. Xue, M. Li, Y. Wang and X. Xu, *Thin Solid Films*, 2009, **517**, 5922; (*b*) U. Lačnjevac, B. M. Jović and V. D. Jović, *Electrochim. Acta*, 2009, **55**, 535; (*c*) F. R. Bento and L. H. Mascaro, *Surf. Coat. Technol.*, 2006, **201**, 1752; (*d*) J. L. Delplancke, J. Dille, J. Reisse, G. J. Long, A. Mohan and F. Grandjean, *Chem. Mater.*, 2000, **12**, 946.
10 (*a*) I. Ban, M. Drofenik and D. Makovec, *J. Magn. Magn. Mater.*, 2006, **307**, 250; (*b*) M. Mandal, D. Pal and K. Mandal, *Colloids Surf., A*, 2009, **348**, 35; (*c*) D. H. Chen and S. H. Wu, *Chem. Mater.*, 2000, **12**, 1354.
11 (*a*) I. Chicinas, V. Pop and O. Isnard, *J. Magn. Magn. Mater.*, 2002, **242-245**, 885; (*b*) X. Y. Qin, J. G. Kim and J. S. Lee, *Nanostruct. Mater.*, 1999, **11**, 259; (*c*) V. V. Tcherdyntsev, S. D. Kaloshkin, I. A. Tomilin, E. V. Shelekhov and Y. V. Baldokhin, *Nanostruct. Mater.*, 1999, **12**, 139.
12 M. Bahgat, M. K. Peak and J. J. Pak, *J. Alloys Compd.*, 2008, **466**, 59.
13 (*a*) X. W. Wei, G. X. Zhu, J. H. Zhou and H. Q. Sun, *Mater. Chem. Phys.*, 2006, **100**, 481; (*b*) X. G. Lu, G. Y. Liang and Y. M. Zhang, *Mater. Sci. Eng., B*, 2007, **139**, 124; (*c*) S. Bai, X. Shen, G. Zhu, Z. Xu and J. Yang, *CrystEngComm*, 2012, **14**, 1432.
14 J. H. Kim, J. Kim, S. K. Lim, C. K. Kim and C. S. Yoon, *J. Magn. Magn. Mater.*, 2007, **310**, 2402.
15 J. L. H. Chau, *Mater. Lett.*, 2007, **61**, 2753.
16 (*a*) X. M. Zhou and X. W. Wei, *Cryst. Growth Des.*, 2009, **9**, 7; (*b*) Q. Liao, R. Tannenbaum and Z. L. Wang, *J. Phys. Chem. B*, 2006, **110**, 14262; (*c*) L. Liu, J. Guan, W. Shi, Z. Sun and J. Zhao, *J. Phys. Chem. C*, 2010, **114**, 13565.
17 (*a*) W. H. Chiang, M. Sakr, X. P. A. Gao and R. M. Sankaran, *ACS Nano*, 2009, **3**, 4023; (*b*) Y. H. Tee, E. Grulke and D. Bhattacharyya, *Ind. Eng. Chem. Res.*, 2005, **44**, 7062; (*c*) B. Schrick, J. L. Blough, A. D. Jones and T. E. Mallouk, *Chem. Mater.*, 2002, **14**, 5140; (*d*) A. D. Bokare, R. C. Chikate, C. V. Rode and K. M. Paknikar, *Environ. Sci. Technol.*, 2007, **41**, 7437.
18 (*a*) Y. D. Li, L. Q. Li, H. W. Liao and H. R. Wang, *J. Mater. Chem.*, 1999, **9**, 2675; (*b*) L. P. Zhu, W. D. Zhang, H. M. Xiao, Y. Yang and S. Y. Fu, *J. Phys. Chem. C*, 2008, **112**, 10073; (*c*) H. L. Niu, Q. W. Chen, Y. S. Lin, Y. S. Jia, H. F. Zhu and M. Ning, *Nanotechnology*, 2004, **15**, 1054; (*d*) X. W. Wei, X. M. Zhou, K. L. Wu and Y. Chen, *CrystEngComm*, 2011, **13**, 1328; (*e*) M. J. Hu, B. Lin and S. H. Yu, *Nano Res.*, 2008, **1**, 303; (*f*) M. J. Hu, Y. Lu, S. Zhang, S. R. Guo, B. Lin, M. Zheng and S. H. Yu, *J. Am. Chem. Soc.*, 2008, **130**, 11606; (*g*)

L. P. Zhu, H. M. Xiao and S. Y. Fu, *Eur. J. Inorg. Chem.*, 2007, 3947; (*h*) Q. Wang, A. Wu, L. Yu, Z. Liu, W. Xu and H. Yang, *J. Phys. Chem. C*, 2009, **113**, 19875; (*i*) M. Cheng, M. Wen, S. Zhou, Q. Wu and B. Sun, *Inorg. Chem.*, 2012, **51**, 1495.

19 (*a*) X. B. Su, H. G. Zheng, Z. P. Yang, Y. C. Zhu and A. L. Pan, *J. Mater. Sci.*, 2003, **38**, 4581; (*b*) H. G. Zheng, J. H. Zhen, H. M. Yu, Y. J. Zhang, J. H. Liang and Y. T. Qian, *J. Ustc.*, 1999, **6**, 29.

20 (*a*) A. Corrias and G. Ennas, *Chem. Mater.*, 1993, **5**, 1722; (*b*) S. J. Shin, Y. H. Kim, C. W. Kim, H. G. Cha, Y. J. Kim and Y. S. Kang, *Curr. Appl. Phys.*, 2007, **7**, 404.

21 Z. T. Zhong, D. A. Biom, Z. Gai, J. R. Thompson, J. Shan and S. Dai, *J. Am. Chem. Soc.*, 2003, **125**, 7528.

22 (*a*) X. M. Ni, Q. B. Zhao, Y. F. Zhang and H. G. Zheng, *Eur. J. Inorg. Chem.*, 2007, 422; (*b*) X. H. Liu, R. Yi, Y. T. Wang, G. Z. Qin, N. Zhang and X. G. Li, *J. Phys. Chem. C*, 2007, **111**, 163; (*c*) Y. C. Zhu, H. G. Zheng, Q. Yang, A. L. Pan, Z. P. Yang and Y. T. Qian, *J. Cryst. Growth*, 2004, **260**, 427.

23 (*a*) L. J. Zhao, H. J. Zhang, Y. Xing, S. Y. Song, S. Y. Yu, W. D. Shi, X. M. Guo, J. H. Yang, Y. Q. Lei and F. Cao, *Chem. Mater.*, 2007, **20**, 198; (*b*) Q. Yang, K. B. Tang, C. R. Wang, Y. T. Qian and S. Y. Zhang, *J. Phys. Chem. B*, 2002, **106**, 9227; (*c*) Q. Yang, K. B. Tang, C. R. Wang, C. J. Zhang and Y. T. Qian, *J. Mater. Res.*, 2002, **17**, 1147; (*d*) C. H. An, Y. Jin, K. B. Tang and Y. T. Qian, *J. Mater. Chem.*, 2003, **13**, 301; (*e*) Q. Yang, F. Wang, K. B. Tang, C. R. Wang, Z. W. Chen and Y. T. Qian, *Mater. Chem. Phys.*, 2002, **78**, 495.

24 (*a*) L. Guo, F. Liang, X. Wen, S. Yang, L. He, W. Zheng, C. Chen and Q. Zhong, *Adv. Funct. Mater.*, 2007, **17**, 425; (*b*) N. Wang, X. Cao, D. Kong, W. Chen, L. Guo and C. Chen, *J. Phys. Chem. C*, 2008, **112**, 6613.

25 (*a*) V. Mendelev and A. Ivanov, *J. Magn. Magn. Mater.*, 2005, **289**, 211; (*b*) V. Salgueirino-Maceira, M. A. Correa-Duarte, A. Hucht and M. Farle, *J. Magn. Magn. Mater.*, 2006, **303**, 163.

26 M. B. Tian, *Magnetic Materials*, Tsinghua University Press, Beijing, 2000.

27 Y. Mei, Y. Lu, F. Polzer, M. Ballauff and F. Polzer, *Chem. Mater.*, 2007, **19**, 1062.

28 (*a*) J. Lee, J. C. Park and H. Song, *Adv. Mater.*, 2008, **20**, 1523; (*b*) T. K. Sau, A. Pal and T. Pal, *J. Phys. Chem. B*, 2001, **105**, 9266; (*c*) K. Esumi, K. Miyamoto and T. Yoshimura, *J. Colloid Interface Sci.*, 2002, **254**, 402; (*d*) K. Hayakawa, T. Yoshimura and K. Esumi, *Langmuir*, 2003, **19**, 5517; (*e*) S. Panigrahi, S. Basu, S. Praharaj, S. Pande, S. Jana, A. Pal, S. K. Ghosh and T. Pal, *J. Phys. Chem. C*, 2007, **111**, 4596; (*f*) K. L. Wu, X. W. Wei, X. M. Zhou, D. H. Wu, X. W. Liu, Y. Ye and Q. Wang, *J. Phys. Chem. C*, 2011, **115**, 16268.